Dalton Transactions

PAPER

View Article Online
View Journal | View Issue

Cite this: *Dalton Trans.*, 2016, **45**, 12078

Superstructure formation in $SrBa_8[BN_2]_6$ and $EuBa_8[BN_2]_6$†

Stefan Seidel,‡[a] Tobias Dierkes,‡[b] Thomas Jüstel,*[b] Christopher Benndorf,[a,c] Hellmut Eckert*[c,d] and Rainer Pöttgen*[a]

Received 20th May 2016,
Accepted 1st July 2016

DOI: 10.1039/c6dt02029a

www.rsc.org/dalton

X-ray pure samples of $SrBa_8[BN_2]_6$ and $EuBa_8[BN_2]_6$ were synthesized from appropriate amounts of binary nitrides (Sr_3N_2, Ba_3N_2 and BN in sealed niobium ampoules and EuN, Ba_3N_2 and BN in BN crucibles, respectively) at temperatures up to 1370 K. The structure of $SrBa_8[BN_2]_6$ was refined from single crystal X-ray diffractometer data: $Fd\bar{3}m$, a = 1595.1(1) pm, w$R(F^2)$ = 0.0515, 387 F^2 values and 21 variables. $EuBa_8[BN_2]_6$ has a lattice parameter of 1595.00(9) pm. Both nitridoborates adopt a new 2 × 2 × 2 superstructure variant of the $LiCa_4[BN_2]_3$ type, realized through ordering of vacancies and Sr^{2+} and Eu^{2+} cations, respectively. The structures of $SrBa_8[BN_2]_6$ and $LiCa_4[BN_2]_3$ are related by a group–subgroup scheme. The Sr^{2+}/vacancy ordering leads to an asymmetric coordination (1 × Sr^{2+} and 8 × Ba^{2+} in a distorted, mono-capped square prism) for the $[BN_2]^{3-}$ units with B–N distances of 132 and 136 pm. Vibrational spectra of $SrBa_8[BN_2]_6$ and $EuBa_8[BN_2]_6$ confirm the discrete linear $[BN_2]^{3-}$ units and ^{11}B solid state MAS NMR spectra are compatible with single crystallographic sites for the boron atoms. In $EuBa_8[BN_2]_6$ the spectra are profoundly influenced by interactions of the ^{11}B nuclei with the unpaired electrons of the paramagnetic Eu^{2+} ions.

1. Introduction

The $[BN_2]^{3-}$ anion is one of the basic building units in nitridoborate crystal chemistry.[1] A first proof for the $[BN_2]^{3-}$ units was obtained by Goubeau and Anselment from IR spectra of $Li_3[BN_2]$, $Ca_3[BN_2]_2$ and $Ba_3[BN_2]_2$,[2] while their precise crystal structures were determined from single crystal X-ray data only much later[3–10] and also the europium compound $Eu_3[BN_2]_2$ was reported.[11,12]

Phase analytical studies later on led to a series of nitridoborate halides $M_2[BN_2]X$ (M = Ca, Sr, Eu; X = F, Cl, Br, I) and $Ba_8[BN_2]_5F$.[13–16] Depending on the metal and halide matrix, the $[BN_2]^{3-}$ units show small distortions, *i.e.* two slightly different B–N distances within the unit and/or N–B–N angles slightly deviating from 180°. Extension of the crystal chemistry is also possible through the ordered replacement of the alkaline earth metal position by alkali or divalent rare earth metals. Many such nitridoborates, $AM_4[BN_2]_3$ (A = Li, Na; M = Ca, Sr, Ba, Eu),[17–21] have been characterized structurally. They are electron-precise nitridoborates with linear $[BN_2]^{3-}$ units. Both series of quaternary nitridoborates have been studied intensively with respect to their IR and Raman spectra.[16,22,23] Distortions (deviations from linearity) of the $[BN_2]^{3-}$ units are readily visible in the IR spectra and the separate bands for the $^{10}B/^{11}B$ isotopologues are resolved. A comparison of the spectra of different compounds reveals a clear correlation between the force constant and the effective partial charge of the $[BN_2]^{3-}$ anion.

Most recent studies on $[BN_2]^{3-}$ containing nitridoborates have concerned their luminescence properties. Polycrystalline samples of $Mg_3[BN_2]N$,[24] $Mg_{8-x}M_x[BN_2]_2N_4$ (M = Al, Si; x = 1, 2)[25] and $Mg_3Ga[BN_2]N$[26] were studied with and without Eu^{2+} doping. These compounds show broad emission bands with orange-red to deep-red photoluminescence. In view of these interesting results we extended our work to the doping of compounds with the composition $MBa_8[BN_2]_6$ (M = Sr, Eu). The structures of both nitridoborates show a 50% occupancy of the strontium/europium site in order to account for an electron precise composition.[27] X-ray powder patterns of our first samples always showed additional reflections that could not be indexed on the basis of the body-centered cell, indicating superstructure formation. Herein we report on a single crystal

[a]*Institut für Anorganische und Analytische Chemie, Universität Münster, Corrensstrasse 30, D-48149 Münster, Germany. E-mail: pottgen@uni-muenster.de; Fax: +49 251-83-36002*
[b]*Fachbereich Chemieingenieurwesen, Fachhochschule Münster, Stegerwaldstraße 39, 48565 Steinfurt, Germany. E-mail: tj@fh-muenster.de*
[c]*Institut für Physikalische Chemie, Universität Münster, Corrensstrasse 30, D-48149 Münster, Germany*
[d]*Institute of Physics in Sao Carlos, University of Sao Paulo, Sao Carlos, SP 13560-590, Brazil. E-mail: eckerth@uni-muenster.de*
†Electronic supplementary information (ESI) available. See DOI: 10.1039/C6DT02029A
‡These authors contributed equally to this work.

study, revealing complete strontium/vacancy ordering within a 2 × 2 × 2 superstructure cell.

2. Experimental

Synthesis

$SrBa_8[BN_2]_6$ was prepared by solid state reaction of stoichiometric quantities of Sr_3N_2 (Materion, 99.5%), Ba_3N_2 (Materion, 99.7%) and h-BN (Alfa Aesar, 99.5%). The binary nitrides were thoroughly ground in an agate mortar and arc-welded[28] in a niobium container under 800 mbar of argon, which was purified by a titanium sponge at 870 K, silica gel and molecular sieves. Subsequently, the niobium container was sealed in an evacuated silica tube for oxidation protection and heated at 1370 K for two hours, followed by slow cooling to room temperature at a rate of 20 K h^{-1}. The slightly yellowish sample was well crystallized and contained small transparent single crystalline platelets suitable for structure determination.

EuN, Ba_3N_2 and BN were used in stoichiometric ratios for the synthesis of polycrystalline $EuBa_8[BN_2]_6$. EuN was synthesized from europium metal (Treibacher, 99.9%), firstly preparing the hydride at 620 K for 2 h in a mixture of argon and hydrogen (Westfalen AG, Ar/W35), followed by subsequent nitridation under N_2 (Westfalen AG, 5.0) at 770 K for 4 h. The starting materials were thoroughly ground in an agate mortar. The mixture was then transferred into BN crucibles, capped with a lid and calcined at 1270 K for 4 h under nitrogen. Both gases were purified using an "oxisorb"-cartridge (Spectron), which reduces the oxygen/moisture level to below five and thirty parts per billion, respectively. Further *in situ* gas purification was carried out using two crucibles filled with Mischmetal placed in front of and behind the reaction vessel. $EuBa_8[BN_2]_6$ was obtained as a dark purple to black polycrystalline powder, similar to $LiEu_4[BN_2]_3$,[21] while the respective Sr compound was almost colorless. Although these two compounds are electron precise, the $[Xe]4f^7$ configuration of Eu^{2+} along with low-lying 4f–5d transitions leads to complete absorption in the visible range. Two broad absorption bands are characteristic of the interconfigurational transition from $[Xe]4f^7$ to $[Xe]4f^65d^1(t_{2g})$ and $[Xe]4f^65d^1(e_g)$ of Eu^{2+} in cubic crystals.[29,30]

Due to the moisture-sensitive nature of the precursors and the final products, all handling was carried out in a nitrogen filled glovebox from GS Glovebox Systemtechnik with H_2O levels well below 50 ppm.

EDX data

The $SrBa_8[BN_2]_6$ single crystal studied on the diffractometer was semi-quantitatively investigated by EDX analyses using a Zeiss EVO® MA10 scanning electron microscope in the variable pressure mode with SrF_2 and BaF_2 as standards. The experimentally observed strontium : barium ratio was 21 ± 2 at % : 79 ± 2 at%, in close agreement with the ideal composition. The light elements could not be analysed owing to the limited instrument resolution. No impurity elements heavier than sodium were observed.

X-ray diffraction

The polycrystalline $SrBa_8[BN_2]_6$ and $EuBa_8[BN_2]_6$ samples were characterized by X-ray powder diffraction using a Guinier camera equipped with an image plate system (Fujifilm, BAS-1800) using $CuK_{\alpha1}$ radiation and α-quartz (a = 491.30, c = 540.46 pm) as an internal standard. The complete patterns could be indexed on the basis of large F-centred cubic cells and least squares refinements resulted in the lattice parameters of a = 1595.1(1) pm for $SrBa_8[BN_2]_6$ and a = 1595.00(9) pm for $EuBa_8[BN_2]_6$. Correct indexing of the patterns was ensured through intensity calculations using the LazyPulverix routine.[31] The powder pattern of $SrBa_8[BN_2]_6$ is exemplarily presented in Fig. 1. The corresponding pattern of the europium compound is available in the ESI.†

Irregularly shaped crystal fragments of $SrBa_8[BN_2]_6$ were glued to thin silica fibers using beeswax. The sample was previously coated with paraffin oil (dried over sodium granules) for protection from hydrolysis. Subsequently the quality of the selected fragments was tested using Laue photographs on a Buerger camera (white molybdenum radiation, the image plate technique, Fujifilm, BAS-1800). Suitable crystals of $SrBa_8[BN_2]_6$ were stored in Schlenk tubes under an argon atmosphere prior to the data collection. Intensity data of the selected crystal were collected at room temperature under a constant nitrogen gas flow using a Stoe StadiVari diffractometer equipped with a Mo microfocus source (λ = 71.073 pm) and a Pilatus 100 K detector with a hybrid-pixel-sensor. A spherical absorption correction was applied to the data set. All relevant crystallographic data and details of the data collection and evaluation are given in Table 1.

Structure refinement

Careful analysis of the $SrBa_8[BN_2]_6$ data set revealed a face-centred cubic lattice and the systematic extinctions were in accordance with space group $Fd\bar{3}m$. The starting atomic para-

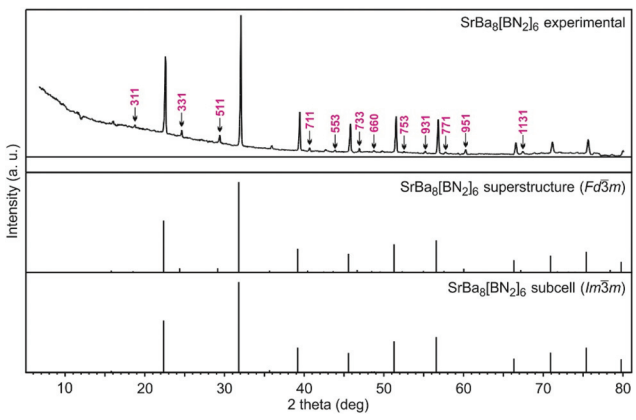

Fig. 1 Experimental (top) and calculated (middle and bottom) X-ray powder patterns of $SrBa_8[BN_2]_6$. The *hkl* indices of the superstructure reflections are marked in the experimental pattern.

Table 1 Crystallographic data and structure refinement for $SrBa_8[BN_2]_6$, space group $Fd\bar{3}m$, $Z = 8$

Formula	$SrBa_8[BN_2]_6$
Molar mass/g mol^{-1}	1419.3
Lattice parameter/pm (powder data)	a = 1595.1(1)
Cell volume/nm^3	V = 4.0585
Density calc./g cm^{-3}	4.65
Crystal size/μm	30 × 40 × 40
Detector distance/mm	60
Exposure time/s	43
Integr. param. A, B, EMS	7.0; −6.0; 0.030
$h\ k\ l$ range	±23; ±23, ±23
θ_{min}, θ_{max}/°	2.21/32.34
Linear absorption coeff./mm^{-1}	17.9
No. of reflections	23 114
R_{int}	0.0198
No. of independent reflections	387
Reflections used [$I \geq 3\sigma(I)$]	284
F(000), e	4800
R factors $R(F)$/w$R(F^2)$ [$I \geq 3\sigma(I)$]	0.0237/0.0453
R factors $R(F)$/w$R(F^2)$ [all data]	0.0450/0.0515
Data/parameters	387/21
Goodness-of-fit on F^2	0.96
Extinction coefficient	—
Diff. Fourier residues/e$^-$ Å^{-3}	−1.54/1.93

meters for the structure refinement were obtained using the charge-flipping algorithm Superflip.[32] The structure was subsequently refined with anisotropic displacement parameters for all atoms on F^2 using Jana2006.[33] As a check for the correct composition and site assignment, the occupancy parameters for all atoms were refined in separate least-squares cycles. All sites were fully occupied within three standard deviations. The setting of the structure was finally adjusted to that required for the group–subgroup scheme (*vide infra*). The final difference Fourier syntheses revealed no significant residues. The refined atomic positions, displacement parameters and interatomic distances are given in Tables 2–4.

Further details of the structure refinement may be obtained from the Fachinformationszentrum Karlsruhe, D-76344 Eggenstein-Leopoldshafen (Germany), by quoting Registry No. CSD-431340.

IR and Raman spectroscopy

For infrared (IR) spectroscopy, KBr specimens were prepared and analysed in the range of 450–2000 cm^{-1} employing a Spectrum 100 FT-IR spectrometer from Perkin Elmer equipped with the Spectrum 6.0.1 data processing software. The Raman spectrum of $SrBa_8[BN_2]_6$ was recorded using a Jobin Yvon HR 800 dispersive Raman spectrometer equipped with a green Nd:YAG laser (λ = 532 nm; P = 20 mW).

Table 2 Atom positions and equivalent isotropic displacement parameters (pm^2) for $SrBa_8[BN_2]_6$. U_{eq} is defined as one-third of the trace of the orthogonalized U_{ij} tensor

Atom	Wyckoff position	X	y	z	U_{eq}
Sr	8a	1/8	1/8	1/8	134(2)
Ba1	32e	0.25833(2)	x	x	230(1)
Ba2	16c	0	0	0	251(1)
Ba3	16d	1/2	1/2	1/2	244(1)
B	48f	0.3671(6)	1/8	1/8	240(30)
N1	48f	0.0344(5)	3/8	3/8	243(15)
N2	48f	0.2025(5)	3/8	3/8	257(15)

Table 3 Anisotropic displacement parameters (pm^2) for $SrBa_8[BN_2]_6$. Coefficients U_{ij} of the anisotropic displacement factor tensor of the atoms are defined by: $-2\pi^2[(ha^*)^2U_{11} + \cdots + 2hka^*b^*U_{12}]$

Atom	U_{11}	U_{22}	U_{33}	U_{12}	U_{13}	U_{23}
Sr	134(4)	U_{11}	U_{11}	0	0	0
Ba1	230(2)	U_{11}	U_{11}	−23(1)	U_{12}	U_{12}
Ba2	250(2)	U_{11}	U_{11}	−61(2)	U_{12}	U_{12}
Ba3	244(2)	U_{11}	U_{11}	−22(2)	U_{12}	U_{12}
B	360(70)	180(30)	U_{22}	0	0	140(30)
N1	170(30)	280(20)	U_{22}	0	0	20(30)
N2	170(30)	300(20)	U_{22}	0	0	−10(30)

Table 4 Interatomic distances (pm) for $SrBa_8[BN_2]_6$

Sr:	6	N1	254.3(8)	N1:	1	B	132(1)
Ba1:	3	N2	277.8(3)		1	Sr	254.3(8)
	3	N1	303.6(1)		2	Ba2	287.3(2)
Ba2:	6	N1	287.3(2)		2	Ba1	303.6(1)
Ba3:	6	N2	292.0(2)	N2:	1	B	136(1)
B:	1	N1	132(1)		2	Ba1	277.8(3)
	1	N2	136(1)		2	Ba3	292.0(2)

Solid state MAS NMR spectroscopy

^{11}B solid state MAS NMR spectra were recorded at magnetic field strengths of 4.7 and 11.7 T on NMR spectrometers at resonance frequencies of 64.166 and 160.419 MHz, respectively, using a Bruker DSX 500 spectrometer. Finely powdered nitridoborates were filled into ZrO_2 MAS rotors with 4 mm diameter and spun at a frequency of 12 kHz with nitrogen gas flow to prevent hydrolysis. Chemical shifts were referenced to $BF_3{\cdot}OEt_2$ as the reference sample; π/2 pulse lengths of p_1 = 3.25–3.80 μs and a relaxation delay of d_1 = 5 s were used in conventional single-pulse experiments. The spectra were recorded using the Bruker Topspin software[34] and analyzed with the *Dmfit* software package.[35] The experimental results are given in Table 7.

3. Crystal chemistry

First hints for superstructure formation were already evident from the Guinier powder patterns which revealed weak additional reflections. The latter could be completely indexed with the 2 × 2 × 2 superstructure cell for both compounds. As an example, the strongest superstructure reflections for $SrBa_8[BN_2]_6$ are marked with small arrows in Fig. 1. The Guinier pattern of $EuBa_8[BN_2]_6$ also shows all of the expected strong superstructure reflections so that both compounds can be considered isotypic. Crystal chemical details of the subcell structure have repeatedly been reported.[17–21] Herein we focus

only on the crystal chemical discussion of the $SrBa_8[BN_2]_6$ superstructure which was refined from single crystal data.

The reason for superstructure formation lies in the electron-precise formulation. When sodium in the alkali metal compound $NaBa_4[BN_2]_3$ [18] is substituted by strontium, charge balance requires half of the strontium sites to remain unoccupied. A view of the $SrBa_8[BN_2]_6$ unit cell is presented in Fig. 2. The strontium-vacancy ordering is not simply realized through decentering of the body-centred cell (as is the case for the well-known example *bcc vs.* CsCl type[36]). The eight subcell strontium sites (50% occupied) around each strontium atom are ordered 4 + 4 in the superstructure, with both strontium and vacancies in a tetrahedral arrangement. This results in a doubling of the subcell in all three directions.

The resulting near-neighbor coordination for the strontium atoms and the $[BN_2]^{3-}$ units is presented in Fig. 3. The strontium atoms have end-on octahedral coordination by $[BN_2]^{3-}$ units with Sr–N distances of 254 pm, similar to the shorter Sr–N distances in the structures of Sr_4N_3 (255–258 pm),[37] SrN (258–265 pm)[38] and $Sr_2Si_5N_8$ (254–272 pm).[39]

The most pronounced influence of the strontium-vacancy ordering is readily seen in the near-neighbor coordination of the $[BN_2]^{3-}$ units. In alkali metal compounds like $NaBa_4[BN_2]_3$,[18] each $[BN_2]^{3-}$ unit has a cation coordination in the form of a bi-capped square prism. Since only half of these sites are filled in the present strontium compound, only the N1 atoms have a strontium neighbor. Consequently we observe a lower number of cations coordinating with the N2 atoms, leading to drastically shortened N2–Ba distances of 278 and 292 pm as compared to the N1–Ba distances of 287 and 304 pm. The barium displacements are readily evident from Fig. 2.

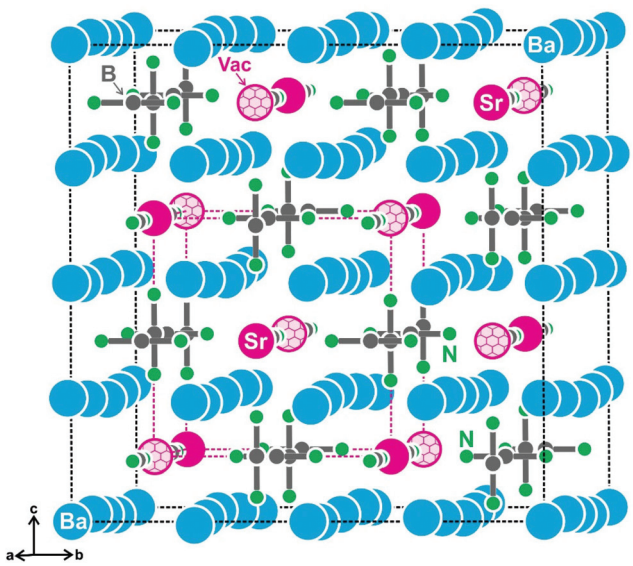

Fig. 2 The unit cell of $SrBa_8[BN_2]_6$. Strontium, barium, boron, and nitrogen atoms are drawn as magenta, blue, grey, and green circles, respectively. The $[BN_2]^{3-}$ units are emphasized and ordered strontium vacancies are marked by honeycomb nets.

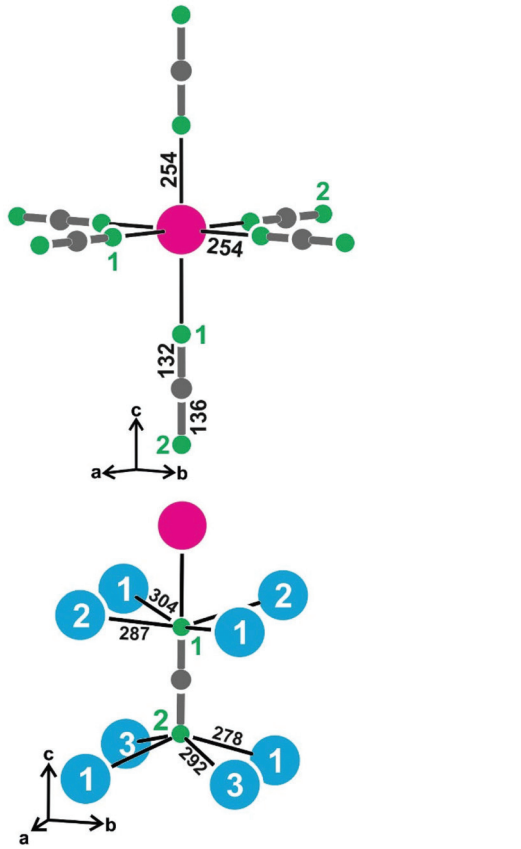

Fig. 3 Near-neighbor coordination of the strontium atoms and the $[BN_2]^{3-}$ units in the structure of $SrBa_8[BN_2]_6$. Strontium, barium, boron, and nitrogen atoms are drawn as magenta, blue, grey, and green circles, respectively. Relevant interatomic distances (pm) and atom designations are given.

The cation ordering leads to asymmetric (but linear) $[BN_2]^{3-}$ units with interatomic distances of 132 pm for B–N1 and 136 pm for B–N2.

We have further analyzed the superstructure model of $SrBa_8[BN_2]_6$ through calculations of the bond valence sums (BVS)[40] and the Chardi algorithm.[41,42] The refined numerical values are listed atom by atom in Table 5. The BVS data result from empirical parameters[43,44] and show strong overbonding for the strontium atoms and strong underbonding for the Ba3 atoms. The charges are much better reproduced with the point-charge approach in Chardi, nicely underlining the elec-

Table 5 Charge distribution analysis of $SrBa_8[BN_2]_6$ using bond valence sums (BVS) and the Chardi algorithm

	Sr	Ba1	Ba2	Ba3	B	N1	N2
$\sum Q$ (BVS)[40]	2.57	1.96	2.02	1.78	2.85	−3.04	−2.81
$\sum Q$ (Chardi)[41]	1.92	2.03	1.92	2.09	2.99	−3.13	−2.87

$BV = e^{(r_0-r)/b}$; b = 0.37, r_0 (Sr^{II}–N) = 223 pm, r_0 (Ba^{II}–N) = 247 pm and r_0 (B^{III}–N) = 147 pm.[43,44]

tron-precise description. This holds also for the covalently bonded $[BN_2]^{3-}$ units.

The $SrBa_8[BN_2]_6$ structure is related with the $LiCa_4[BN_2]_3$ subcell type through a group–subgroup relation, which is presented in the Bärnighausen formalism[45–47] in Fig. 4. The symmetry reduction proceeds in two steps. First we observe a decentering of the body-centred lattice through a *klassengleiche* transition of index 2 (k2) from $Im\bar{3}m$ to $Pn\bar{3}m$. Although this symmetry reduction leads to splitting of the 8*c* calcium site, there is still no possibility of ordering of the strontium atoms for the title compound. Subsequently, a second *klassengleiche* transition of index 2 (k2) from $Pn\bar{3}m$ to $Fd\bar{3}m$ upon doubling of the unit cell in all three directions proceeds and the splitting of the 2*a* site into two eightfold sites in the superstructure allows for strontium-vacancy ordering. The *klassengleiche* transitions lead to the superstructure reflections observed in the powder patterns. The symmetry reductions also lead to free *x* parameters for the Ba1 and B atoms as well as two different *x* parameters for N1 and N2.

Ordering of cation vacancies has also been determined for the β-$Ca_3[BN_2]_2$ structure,[7] but with a different symmetry reduction. This superstructure variant crystallizes with the orthorhombic space group *Cmce*. The smaller calcium atoms and the different pattern of vacancy ordering lead to significant tilts and bending of the $[BN_2]^{3-}$ units. For comparison, projections of the $SrBa_8[BN_2]_6$ and β-$Ca_3[BN_2]_2$ structures are presented in Fig. 5.

4. Vibrational spectroscopy

Linear $[BN_2]^{3-}$ nitridoborate anions are the characteristic structural units of $SrBa_8[BN_2]_6$ and $EuBa_8[BN_2]_6$. The numerous vibrational modes can be easily detected in either IR and/or Raman spectra. The actual number of modes that can be expected in the solid, dependent on the exact symmetry of the dumbbell-shaped $[BN_2]^{3-}$ units, has been discussed in detail before for several similar compounds.[2,9,12,23,48] Fig. 6 depicts the IR spectra of $SrBa_8[BN_2]_6$ and $EuBa_8[BN_2]_6$. The two isotypic nitridoborates exhibit almost identical spectra. The numerical values of the frequencies are listed in Table 6. IR-active, characteristic anti-symmetric stretching modes υ_2 of the B–N bonds can be observed in the range between 1600 and 1700 cm^{-1} (band splitting is a consequence of factor group splitting) and lower-lying doubly degenerate deformation modes υ_3 from 500 to 650 cm^{-1}. Additional splitting of bands is due to the presence of ^{11}B and ^{10}B isotopologues at the natural abundance ratio of 80 : 20. The assumption of asym-

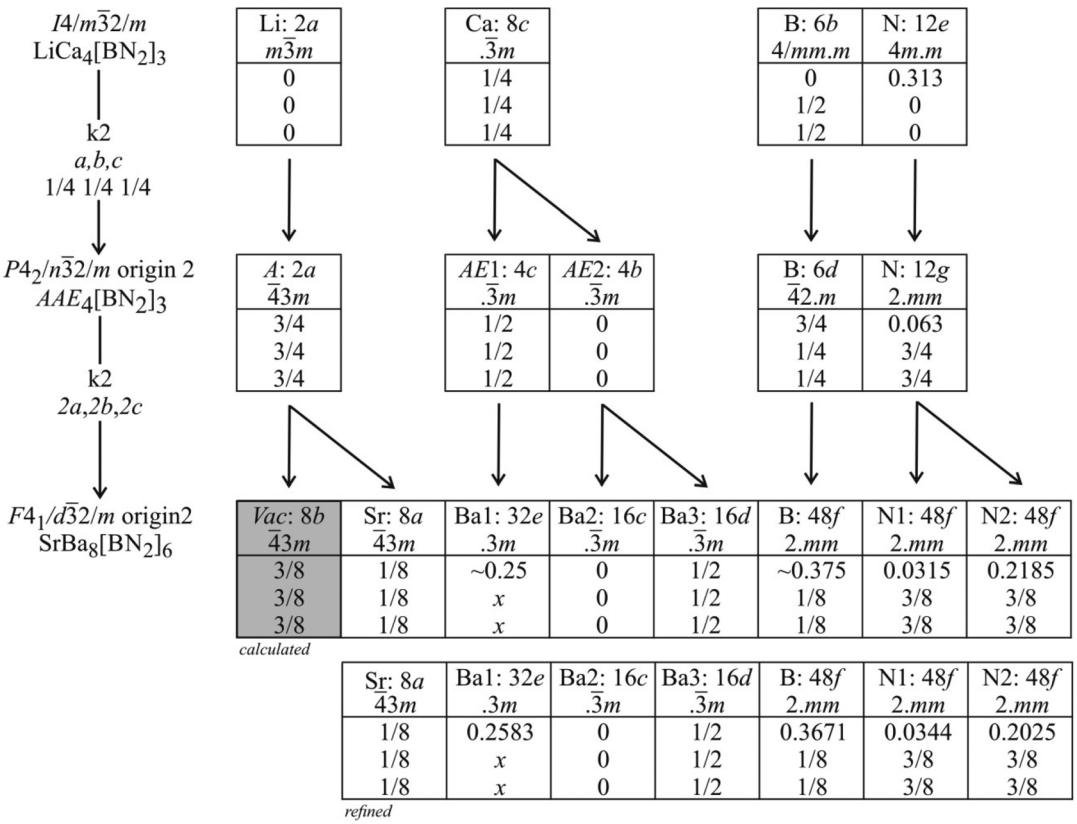

Fig. 4 Group–subgroup scheme in the Bärnighausen formalism[45–47] for the structures of $LiCa_4[BN_2]_3$ and $SrBa_8[BN_2]_6$. The indices for the *klassengleiche* (k) symmetry reductions, the unit cell transformations, and the evolution of the atomic parameters are given. No representative is known for the intermediate space group $Pn\bar{3}m$. The alkali and alkaline earth sites for that intermediate are symbolized by *A* and *AE*, respectively.

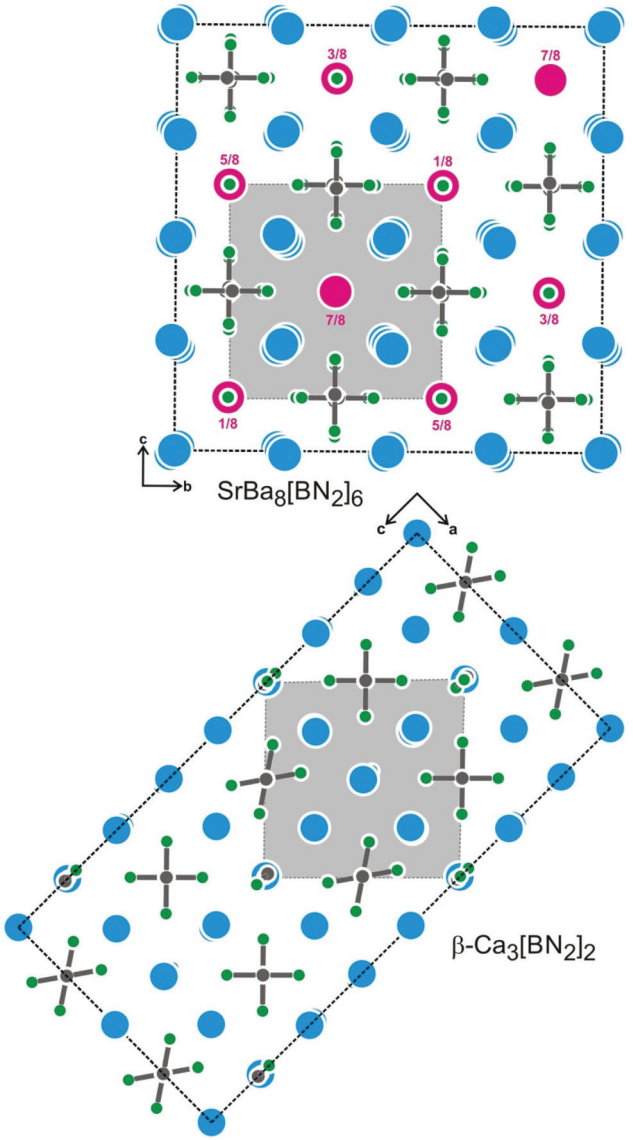

Fig. 5 Projections of the $SrBa_8[BN_2]_6$ and β-$Ca_3[BN_2]_2$ structures. Heights of the strontium atoms in $SrBa_8[BN_2]_6$ are indicated. Both superstructures are a consequence of vacancy ordering. For further details of the vacancy ordering in β-$Ca_3[BN_2]_2$, we refer the reader to ref. 7.

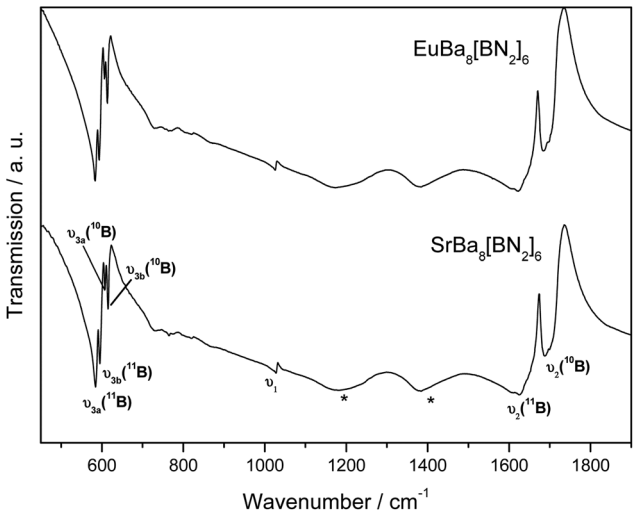

Fig. 6 IR spectra of $SrBa_8[BN_2]_6$ and $EuBa_8[BN_2]_6$. Relevant modes are indicated. For numerical values see Table 6. The modes marked with asterisks result from slow decomposition of the samples.

Table 6 Frequencies (cm^{-1}) of the fundamental modes of the IR spectra (Fig. 6) of $SrBa_8[BN_2]_6$ and $EuBa_8[BN_2]_6$

	υ_1	υ_2 (^{11}B)	υ_2 (^{10}B)	υ_{3a} (^{11}B)	υ_{3b} (^{11}B)	υ_{3a} (^{10}B)	υ_{3b} (^{10}B)
$SrBa_8[BN_2]_6$	1028	1625	1687	585	595	607	615
$EuBa_8[BN_2]_6$	1025	1622	1684	583	593	606	613

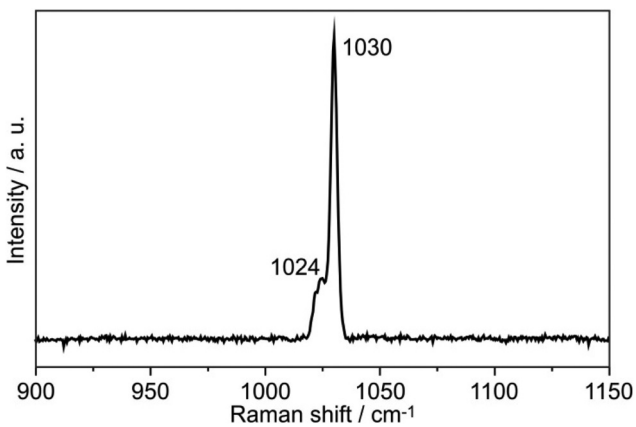

Fig. 7 Raman spectrum of $SrBa_8[BN_2]_6$.

metric $[BN_2]^{3-}$ units as confirmed by the crystallographic data is underlined by the presence of the symmetric ν_1 stretching mode in the FTIR spectrum. Further confirmation of the broken linear symmetry, due to different B–N bond lengths, is given by the doublet splitting of the ν_3 deformation modes.

The Raman spectrum of $SrBa_8[BN_2]_6$ is presented in Fig. 7. $EuBa_8[BN_2]_6$ was also tested; however, similarly to $LiEu_4[BN_2]_3$ [23] it decomposed during laser exposure. The symmetric B–N stretching splits into two bands in the Raman spectrum at 1024 and 1030 cm^{-1}, similar to the situation in $Ca_3[BN_2]I$[48] that also shows two different B–N bond lengths of 139.3 and 136.9 pm.

5. ^{11}B solid state MAS NMR spectroscopy

The ^{11}B solid state MAS NMR spectra of the nitridoborates $SrBa_8[BN_2]_6$ and $EuBa_8[BN_2]_6$ are shown in Fig. 8 and 9, respectively. Consistent with the crystal structure the spectra show only one signal whose line shape is strongly influenced by second order quadrupolar perturbations induced by the

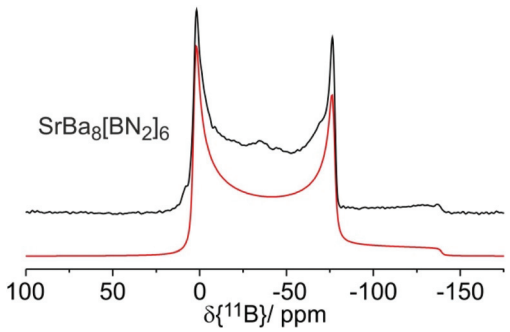

Fig. 8 ^{11}B MAS NMR spectrum of $SrBa_8[BN_2]_6$ with simulation (red line) recorded at an external magnetic flux density of B_0 = 4.7 T and a spinning frequency of 12 kHz.

Table 7 ^{11}B NMR spectroscopic parameters of the nitridoborates $SrBa_8[BN_2]_6$ and $EuBa_8[BN_2]_6$: isotropic resonance shifts δ_{iso} (±1 ppm), quadrupolar coupling constant C_Q (±0.05 MHz) and electric field gradient asymmetry parameter η_{CQ} (±0.03), magnetic flux density of external field B_0 (T) and line broadening parameter LB (±1.0 ppm)

	δ_{iso}	C_Q	η_{CQ}	B_0	LB
$SrBa_8[BN_2]_6$	26.6	3.30	0.02	4.7	2.0
$EuBa_8[BN_2]_6$	26.6	3.10	0.03	4.7	15.2
	24.3	3.10	0.03	11.7	7.0

interaction of the ^{11}B nuclei with the electric field gradient resulting from their non-spherical electronic environment. Table 7 summarizes the quadrupolar coupling constant C_Q and the asymmetry parameter η_Q obtained by fitting the line shape of the central transition. Consistent with the $C_{\infty v}$ local symmetry at the boron site, the field gradient is found to be close to axially symmetric in both compounds. The spectra of the Eu^{2+} compound are profoundly influenced by the proximity of the unpaired 4f-electrons to the ^{11}B nuclei. This *paramagnetic interaction* manifests itself in (1) a broadening effect imposed on the second-order quadrupolar powder pattern characterizing the central 1/2 ↔ −1/2 transition and (2) the appearance of intense MAS sidebands, reflecting strong inhomogeneous spectral broadening effects. The latter arise from the anisotropic effective local field generated at the site of the ^{11}B nuclei by proximal electron spins, which are rapidly fluctuating between their Zeeman states. For the quadrupolar ^{11}B nuclei this interaction is superimposed on the anisotropy of the nuclear electric quadrupolar interaction affecting the ±1/2 ↔ ±3/2 "satellite" Zeeman transitions. Fig. 9 shows the spinning sideband profiles at the external magnetic flux densities of 4.7 and 11.7 T. A detailed analysis of these sideband profiles requires additional experimental inputs from EPR spectroscopy and will be presented in a forthcoming study.

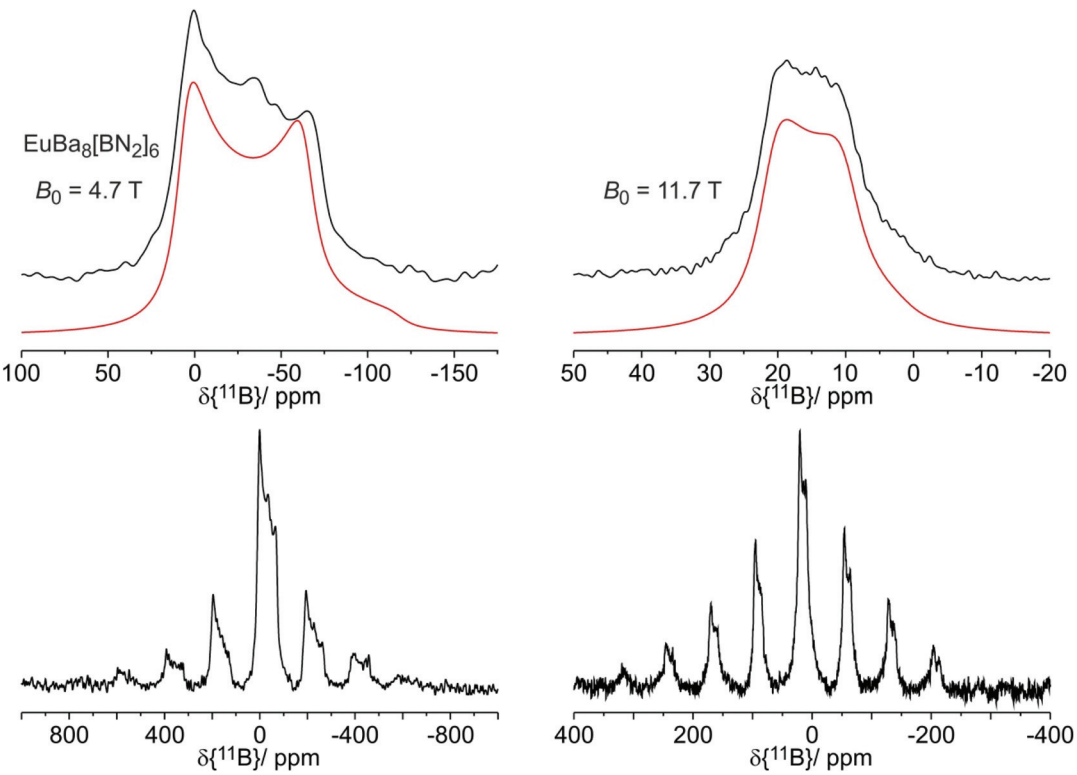

Fig. 9 Enlarged ^{11}B MAS NMR spectra of $EuBa_8[BN_2]_6$ recorded at external magnetic flux densities of B_0 = 4.7 T (top left) and B_0 = 11.7 T (top right) with simulated spectra (red lines) and full spectra with spinning side-band patterns (bottom).

6. Conclusions and outlook

High-resolution powder and single crystal X-ray diffraction data confirm full cation ordering in the nitridoborates $SrBa_8[BN_2]_6$ and $EuBa_8[BN_2]_6$. Both compounds crystallize with a new superstructure that derives from the $LiCa_4[BN_2]_3$ type through a group–subgroup scheme. The cation ordering leads to asymmetric linear $[BN_2]^{3-}$ units with B–N distances of 132 and 136 pm. This is underlined by vibrational spectroscopy. The ^{11}B solid state MAS NMR spectra confirm the presence of single boron atomic sites in both compounds, whose electronic environment is characterized by axially symmetric electric field gradients. The spectrum of the Eu compound is additionally influenced by strong anisotropic paramagnetic interactions, resulting in characteristic field-dependent spectra. $SrBa_8[BN_2]_6$ is an excellent host structure for doping with divalent or trivalent rare earth cations. Detailed optical, solid state NMR and ESR studies will be published shortly.

Acknowledgements

We thank Dipl.-Ing. U. Ch. Rodewald for the collection of the single crystal intensity data.

References

1 B. Blaschkowski, H. Jing and H.-J. Meyer, *Angew. Chem., Int. Ed.*, 2002, **41**, 3322–3336.
2 J. Goubeau and W. Anselment, *Z. Anorg. Allg. Chem.*, 1961, **310**, 248–260.
3 H. Yamane, S. Kikkawa, H. Horiuchi and M. Koizumi, *J. Solid State Chem.*, 1986, **65**, 6–12.
4 H. Yamane, S. Kikkawa and M. Koizumi, *J. Solid State Chem.*, 1987, **71**, 1–11.
5 R. C. DeVries and J. F. Fleischer, *Mater. Res. Bull.*, 1969, **4**, 433–441.
6 M. Wörle, H. Meyer zu Altenschildesche and R. Nesper, *J. Alloys Compd.*, 1998, **264**, 107–114.
7 M. Häberlen, J. Glaser and H.-J. Meyer, *J. Solid State Chem.*, 2005, **178**, 1478–1487.
8 H. Womelsdorf and H.-J. Meyer, *Z. Anorg. Allg. Chem.*, 1994, **620**, 262–265.
9 O. Reckeweg, F. J. DiSalvo and M. Somer, *J. Alloys Compd.*, 2003, **361**, 102–107.
10 M. Häberlen, *Synthesen, Kristallstrukturen und Phasenübergänge der Nitridoborate der Erdalkalimetalle*, Dissertation, Universität Tübingen, Germany, 2006.
11 W. Carillo-Cabrera, M. Somer, K. Peters and H. G. von Schnering, *Z. Kristallogr. – New Cryst. Struct.*, 2001, **216**, 43–44.
12 M. Somer, C. Gül, R. Müllmann, B. D. Mosel, R. K. Kremer and R. Pöttgen, *Z. Anorg. Allg. Chem.*, 2004, **630**, 389–393.
13 F. E. Rohrer, *Nitridoborate und Nitridoborat-Halogenide von Erdalkali- und Seltenerdmetallen*, Dissertation 12468, ETH Zürich, Switzerland, 1997.
14 F. E. Rohrer and R. Nesper, *J. Solid State Chem.*, 1999, **142**, 187–191.
15 F. E. Rohrer and R. Nesper, *J. Solid State Chem.*, 1999, **142**, 192–198.
16 I. Kokal, U. Aydemir, Yu. Prots, W. Schnelle, L. Akselrud, P. Höhn and M. Somer, *Z. Kristallogr.*, 2011, **225**, 633–639.
17 M. Somer, U. Herterich, J. Curda, K. Peters and H. G. von Schnering, *Z. Kristallogr.*, 1994, **209**, 182.
18 M. Somer, U. Herterich, J. Curda, K. Peters and H. G. von Schnering, *Z. Kristallogr.*, 1995, **210**, 529.
19 M. Somer, W. Carillo-Cabrera, K. Peters and H. G. von Schnering, *Z. Kristallogr. – New Cryst. Struct.*, 2000, **215**, 209.
20 M. Somer, U. Herterich, J. Curda, K. Peters and H. G. von Schnering, *Z. Kristallogr.*, 1996, **211**, 54.
21 J. Curda, U. Herterich, K. Peters, M. Somer and H. G. von Schnering, *Z. Kristallogr.*, 1994, **209**, 618.
22 M. Somer, *Z. Naturforsch.*, 1991, **46b**, 1664–1668.
23 M. Somer, U. Herterich, J. Čurda, W. Carillo-Cabrera, A. Zürn, K. Peters and H. G. von Schnering, *Z. Anorg. Allg. Chem.*, 2000, **626**, 625–633.
24 J. Schölch, T. Dierkes, D. Enseling, M. Ströbele, T. Jüstel and H.-J. Meyer, *Z. Anorg. Allg. Chem.*, 2015, **641**, 803–808.
25 M. Ströbele, K. Dolabdjian, D. Enseling, D. Dutczak, B. Mihailova, T. Jüstel and H.-J. Meyer, *Eur. J. Inorg. Chem.*, 2015, 1716–1725.
26 D. Dutczak, K. M. Wurst, M. Ströbele, D. Enseling, T. Jüstel and H.-J. Meyer, *Eur. J. Inorg. Chem.*, 2016, 861–866.
27 S. S. Öztürk, I. Kokal and M. Somer, *Z. Kristallogr. – New Cryst. Struct.*, 2005, **220**, 303–304.
28 R. Pöttgen, Th. Gulden and A. Simon, *GIT Labor-Fachz.*, 1999, **43**, 133–136.
29 N. Yamashita, *J. Electrochem. Soc.*, 1993, **140**, 840–843.
30 Y. Nakao, *J. Phys. Soc. Jpn.*, 1980, **48**, 534–541.
31 K. Yvon, W. Jeitschko and E. Parthé, *J. Appl. Crystallogr.*, 1977, **10**, 73–74.
32 L. Palatinus and G. Chapuis, *J. Appl. Crystallogr.*, 2007, **40**, 786–790.
33 V. Petříček, M. Dušek and L. Palatinus, *Z. Kristallogr.*, 2014, **229**, 345–352.
34 Bruker Corporation, *Topspin (Version 2.1)*, Karlsruhe, 2008.
35 D. Massiot, F. Fayon, M. Capron, I. King, S. Le Calvé, B. Alonso, J.-O. Durand, B. Bujoli, Z. Gan and G. Hoatson, *Magn. Reson. Chem.*, 2002, **40**, 70–76.
36 R. Pöttgen, *Z. Anorg. Allg. Chem.*, 2014, **640**, 869–891.
37 Yu. Prots, G. Auffermann, M. Tovar and R. Kniep, *Angew. Chem., Int. Ed.*, 2002, **114**, 2392–2394.
38 G. Auffermann, Yu. Prots and R. Kniep, *Angew. Chem.*, 2001, **113**, 565–567.
39 T. Schlieper, W. Milius and W. Schnick, *Z. Anorg. Allg. Chem.*, 1995, **621**, 1380–1384.
40 I. D. Brown, *Chem. Soc. Rev.*, 1978, **7**, 359–376.

41 R. Hoppe, S. Voigt, H. Glaum, J. Kissel, H. P. Müller and K. Bernet, *J. Less-Common Met.*, 1989, **156**, 105–122.
42 M. Nespolo and B. Guillot, *J. Appl. Crystallogr.*, 2016, **49**, 317–321.
43 I. D. Brown and D. Altermatt, *Acta Crystallogr.*, 1985, **B41**, 244–247.
44 N. E. Brese and M. O'Keeffe, *Acta Crystallogr.*, 1991, **B47**, 192–197.
45 H. Bärnighausen, *Commun. Math. Chem.*, 1980, **9**, 139–175.
46 U. Müller, *Z. Anorg. Allg. Chem.*, 2004, **630**, 1519–1537.
47 U. Müller, *Symmetriebeziehungen zwischen verwandten Kristallstrukturen*, Vieweg + Teubner Verlag, Wiesbaden, 2012.
48 T. Ezgi Toros, M. Yahyaoglu, U. Aydemir, C. Drathen, L. Akselrud, Y. Prots, P. Höhn and M. Somer, *Z. Anorg. Allg. Chem.*, 2015, **641**, 2014–2019.